Lagrangian single-column modeling of Arctic airmass transformation during HALO-($\mathscr{AC}$)^3

Michail Karalis[1,], Gunilla Svensson[1,2], Manfred Wendisch[3], Michael Tjernström[1]

[1]Stockholm University, Department of Meteorology and Bolin Centre for Climate Research, Stockholm, Sweden

[2]KTH Royal Institute of Technology, Department of Engineering Mechanics, FLOW, Stockholm, Sweden

[3]Leipzig Institute for Meteorology (LIM), Leipzig University, Leipzig, Germany

July 23, 2025

We would like to thank the ACP editor and all anonymous referees for their insightful review of the manuscript. Below you may find our responses (regular font text) to each of the referee's remarks (gray text) along with the respective changes made in the manuscript (**"bold text"**)

Referee #2

The paper investigates air mass transformations (radiative, turbulent, clouds, precipitation) associated with Arctic warm air intrusions. The paper is very well written, with a clear and concise introduction highlighting the existing knowledge and gaps in understanding cloud processes and air mass transformations, and presenting important results which advance our understanding of processes associated with warm air intrusions strongly affecting the Arctic climate. My major recommendations are to strengthen the abstract including key conclusions and slightly modify the results section structure to bring forward the air mass transformation processes and drivers, shifting the focus from model intercomparison. Also, the methodology section requires more details about the three models used in the study including relevant parameterizations. Below I provide more details. These are relatively minor revisions to clarify certain interpretations and to strengthen the presentation of the paper. I recommend the paper publication after they are addressed.

We are grateful for the reviewer's positive review and valuable input. Their thorough comments helped enhance the quality of the manuscript considerably.

Abstract: The abstract includes detailed methodology description and however lacking somewhat the main results. It will be beneficial for the paper if the readers could learn from the abstract what are the key conclusions regarding the air mass transformation.

A: Thank you for this comment. We modified the abstract to more clearly feature they key findings of the study by adding the following lines.

L9-12: " Cloud radiative cooling and turbulent mixing in the stably stratified boundary layer are constant sinks of heat throughout the airmass transformation. Boundary layer cooling intensifies over the marginal ice zone and forces the development of a low-level cloud underneath the advected one. As the airmass flows past the marginal ice zone, large-scale

updrafts dominate the temperature and moisture changes through adiabatic cooling and condensation. ”

Data and Methods section: overall it is very clear and well written however some key details regarding observations and models used in the study are missing. In particular:

2.1 Observations: it will be helpful to know more details about the dropsondes (which type, parameters measured directly, vertical resolution, accuracy, etc)

A: Vaisala RD41 dropsondes were used for measuring Temperature, pressure, relative humidty and horizontal wind speed. We specify the dropsonde model in the text and refer to the Vaisala, 2020 datasheet and the HALO-AC3 data overview paper by Ehrlich et al. (2025) for all the relevant technical information. We added:

L87: “equipped with an extensive set of instruments (Ehrlich et al., 2025)”

L89 - 90: “Vaisala RD41 dropsondes **(Vaisala, 2020)”**

L91: “Detailed information on the dropsonde data can be found in Ehrlich et al. (2025).”

2.4 Model description: key details are missing and will be helpful to include in the model description: resolution (ERA5 and IFS), cloud parameterization schemes, convection parameterization, and the snow pack model – in particular, details on how snow on sea ice is represented in the AOSCM.

A: We have added the following lines to

L143-144 “The parameterization schemes for radiation, turbulence, convection and cloud microphysics are described in detail in the IFS cy43r3 documentation (ECMWF, 2017) ”

L145-147 “In our set-up, five thickness categories and two vertical levels are used to describe the sea-ice layer while snow is represented by a singular layer on top of the sea-ice. The LIM3 halo-thermodynamic parameterizations are solved for all categories and levels”

Figure 1 caption: “Isobars between 940 hPa and 1080 hPa are plotted with thin(thick) white lines with a 5(10) hPa step” – while it is obvious from the values, it has to be noted that this is mean sea level pressure. Also, including selected makers on the plots will help

A: We have now specified the use of mean sea level pressure in the figure caption. We find that adding the values on the contours, unfortunately, makes the figure less readable without necessarily adding much valuable information. The configuration of the systems that formed the meridional advection corridor is more relevant than their individual strengths for the subject of this study. We made the contours thicker to enhance readability. The MIZ borders have been redrawn to match the new definition, inspired by the referee’s next comment.

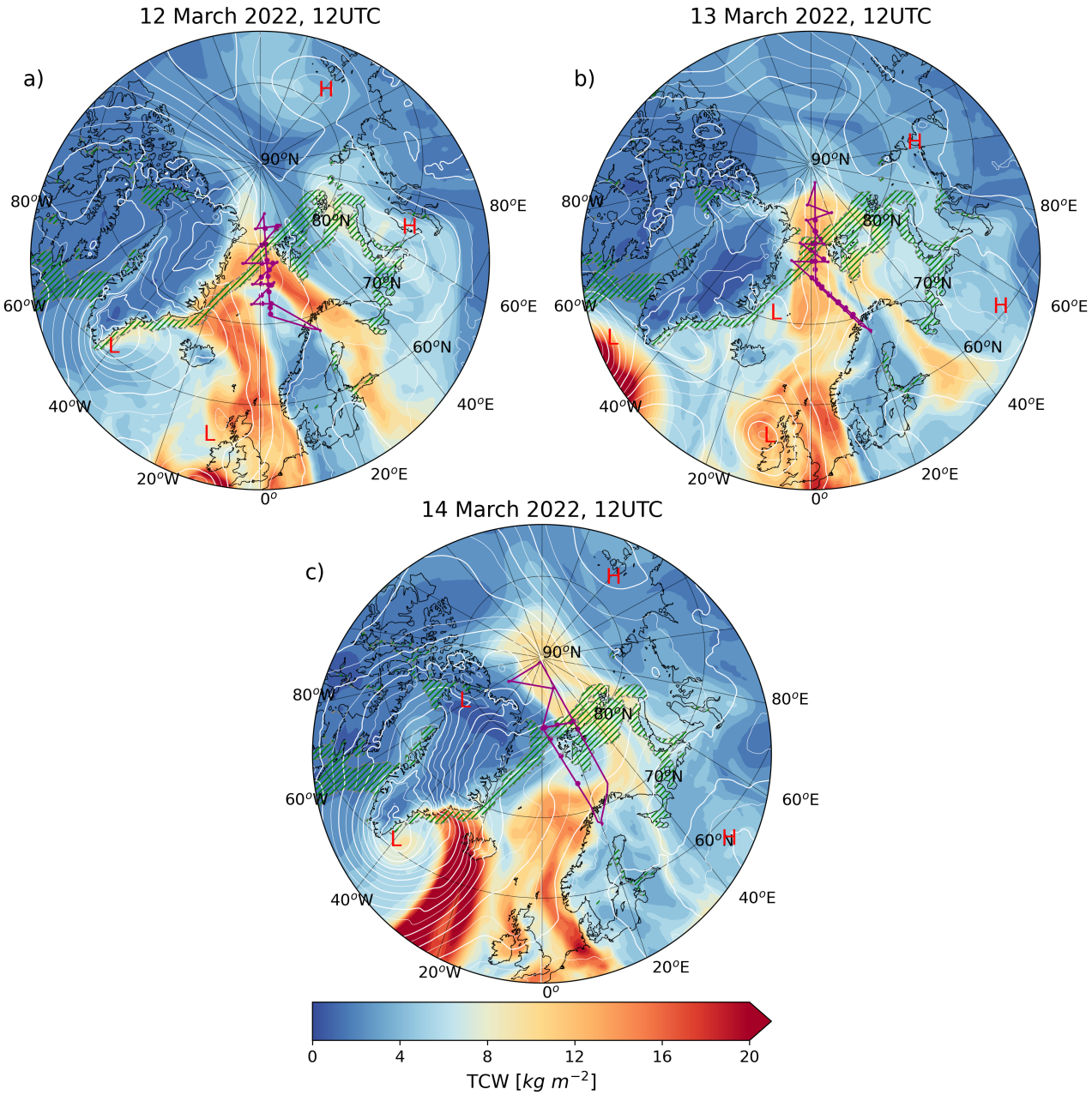

Figure AR2.1: Maps of total column water (kg m–2) at 12 UTC, on each day of the 12-14 March WAI event. **Mean sea level pressure contours** ~~Isobars~~ between 940 hPa and 1080 hPa are plotted with thin(thick) white lines with a 5(10) hPa step. The centers of low and high pressure centers are marked with denoted with red letters. The green hatched area marks the extent of the marginal ice zone (MIZ) which corresponds to sea-ice fraction between values of ~~0~~**0.15** and ~~0.9~~**0.8**. Purple lines represent the respective HALO flight tracks (RF02, RF03, RF04) over the North Atlantic. The purple dots correspond to the locations of dropsondes released during each flight.

Marginal sea ice zone: typically SIC of 80% is used as the upper limit to define MIZ, while the authors used here 90%. Could the authors justify their choice?

A: The definition of the marginal ice zone (MIZ) in our experiments determines the residence time over each surface as well as the representative values for sea-ice concentration and sea-ice and snow thickness of each leg. We initially chose to extend our marginal ice zone (MIZ) definition to include

sea-ice concentrations of 90%, in an effort to account for the contribution of the open water areas more properly.

However, in order to ensure consistency with previous studies and support the broader use of the Lagrangian AOSCM on warm-air intrusion cases in the future, we have redefined the MIZ as the region with 0.15 < sea-ice concentration < 0.8 in our experiments. This change shortens the MIZ leg by approximately three hours. Repeating the simulations with this updated definition produces only minor differences in the overall airmass transformation (Fig. AR2.2). We have now updated all figures and relevant text accordingly.

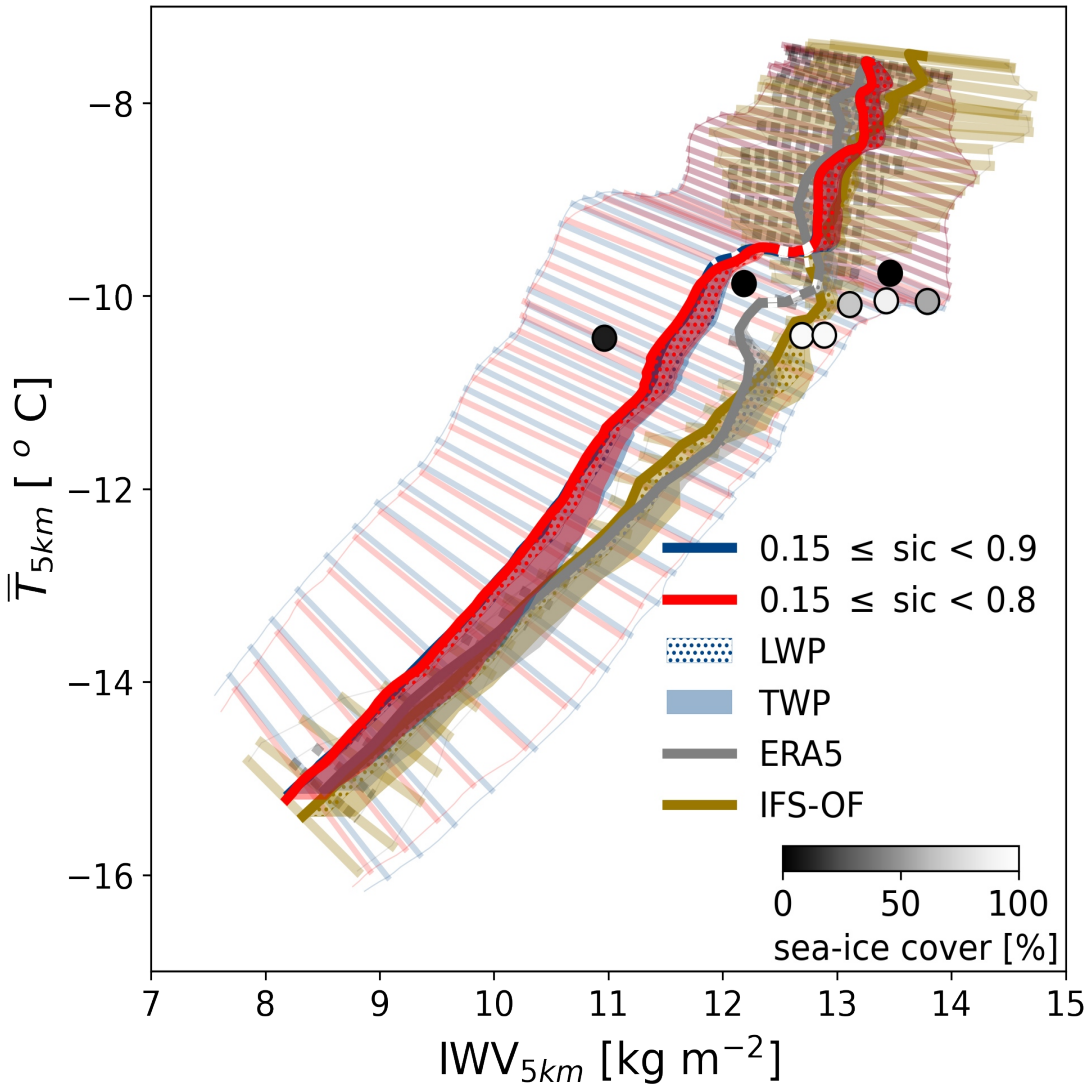

Figure AR2.2: Same as Fig. 4 in the main manuscript but including experiments with different definitions of the MIZ.

Lines 93-94: "On March 13, at 12 UTC we launch 24-hour long trajectories, 600 in total, half of which were computed backward and half forward in time. " – it will be helpful to show on the figure from where the trajectories launched on Fig. 2a (eg, can highlight in bold the 81ºN line portion near the appropriate meridian not to clutter the figure)

A: Thank you for the suggestion. We added a thick line in Fig. 2 along the 81ºN zone to show the latitude of initialization. We reconfigured and enlarged the plots as proposed by Ref #3.

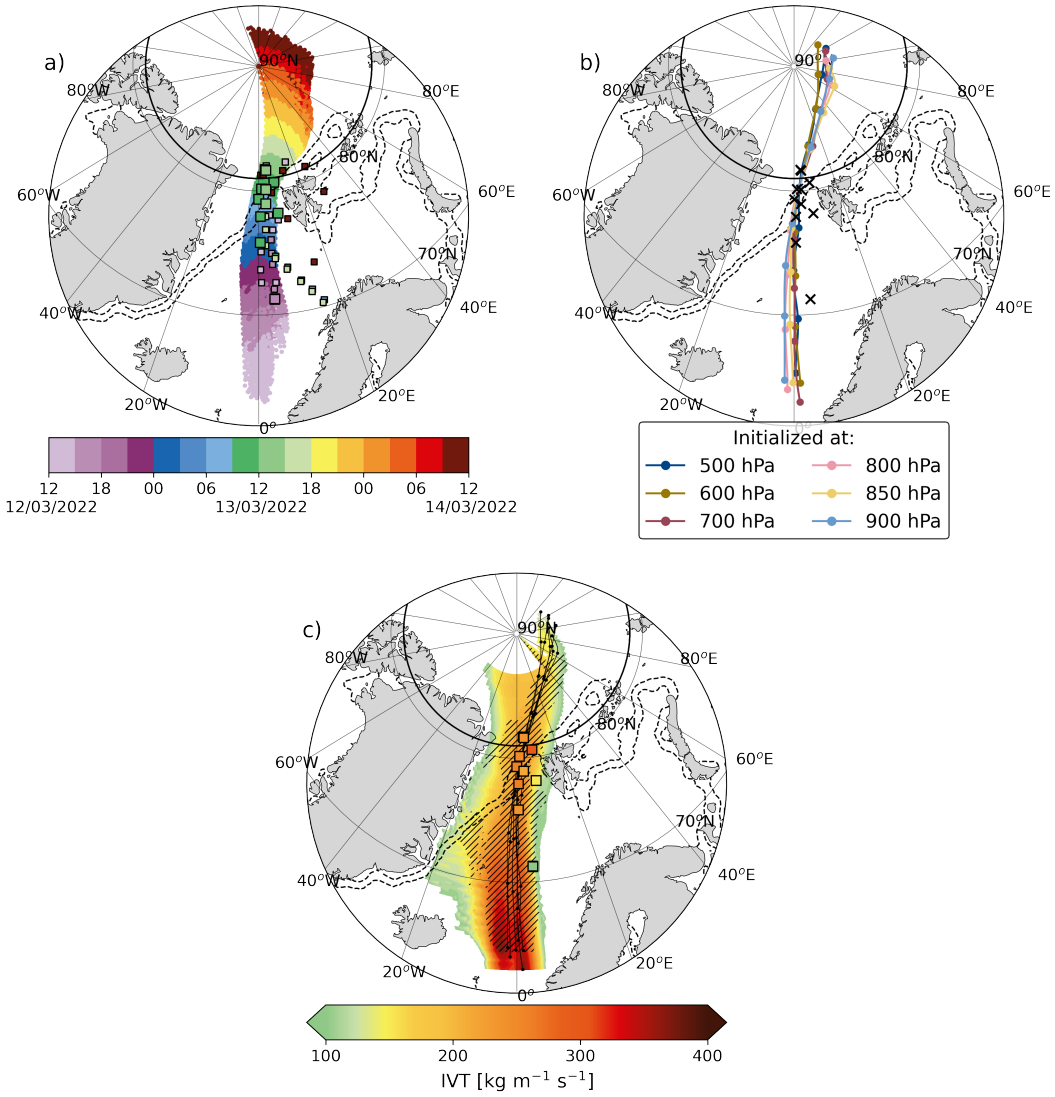

Figure AR2.3: Same as Fig. 2 in the main manuscript.

In the caption, we added the line **"(marked with a thick solid line)"** beside 81° N. We also removed ~~(day of year = 72.5)~~ since it is an unnecessary detail.

Fig 2 c) temporal evolution and spatial variability of integrated water vapor transport (IVT).

Could the authors explain in more detail how IVT temporal evolution is calculated – is it the value for each specific trajectory (which would be difficult given the number of trajectories), along latitudinal line across the trajectory ensemble? Also for trajectories at which level?

A: The trajectories in these plots serve the purpose of a time axis. The trajectory ensemble that we use throughout this study consists of 6 trajectories initialized at 500, 600, 700, 800, 850 and 850 hPa respectively. We follow along each trajectory from south to north and, at each timestep, scan in the

perpendicular direction for IVT values of 100 kg m^{-2} s^{-1}, which is a threshold used for Arctic warm-air intrusion and atmospheric river detection. We repeat the process for all trajectories and present the averaged fields. When examining IVT from this Lagrangian perspective, one can see the width of the airmass and IVT variability in the direction normal to the trajectories and how it evolves in time along the trajectory ensemble.

We rewrote the caption of Fig. 2 to make the method clearer. The new caption is presented below:

"a) 24-hour long backward and forward trajectories initialized at pressure levels (500, 600, 700, 800, 850 and 900 hPa), within a 100 km-radius circle centered on 81 °N (marked with a thick solid line) and 5 °E on 13 March, at 12 UTC. The coloring along the trajectories represents the air-parcels' time of arrival at the marked location. The squares mark the locations of all dropsondes released during flights RF02, RF03 and RF04 and are tinted, similarly to the trajectories, according to the dropsonde launch. Smaller squares are used to denote observations whose location and time of launch constitutes the unfit for comparison with trajectories. Dashed contours show boundaries of the MIZ, corresponding to sea-ice concentration values ~~0~~ **0.15** and ~~0.9~~ **0.8**, at the time of the trajectory initialization. **b)** ~~The trajectory ensemble consisting of one trajectory per pressure level, colored accordingly.~~ **The trajectory ensemble showing the closest vertical alignment. Trajectories are colored according to the pressure they were initialized at.** Dots mark 6 hour long periods. X-shaped markers show the locations of observed profiles suited for comparison. **c)** ~~temporal evolution and spatial variability of integrated water vapor transport (IVT). The trajectory ensemble is shown with black lines. Hatches mark the correlation range (see Sect. 2.3) around the airmass at each timestep.~~ **Map of the temporal evolution and spatial variability of integrated water vapor transport (IVT). The trajectory ensemble, drawn with black lines, serves the purpose of a time axis. IVT changes in the direction parallel to the trajectories show the temporal evolution of the airmass. IVT changes in the direction perpendicular to the trajectories show the spatial variability of the airmass at the respective timestep (12/03/2022 12 UTC at the southernmost point to 14/03/2022 12 UTC at the northernmost). Hatches mark the correlation range showing areas around the trajectories of similar vertical structure at each timestep (see Sect. 2.3). "**

We use the same visualization approach for Fig. 3. We make the following changes in the caption of that figure:

"~~The trajectory ensemble is shown with black lines.~~ **The trajectory ensemble, drawn with black lines, serves the purpose of a time axis, similar to Fig. 2c"**

Lines 106-107: "These are identified using an integrated vapor transport (IVT) threshold of 100 kg m−1 s−1, generally preferred for Arctic WAI and AR detection " – I suggest adding also an Arctic-focused paper, eg Viceto et al (2022), and a polar-focused reference by Zhang et al (2024) where specific thresholds are mentioned:

Viceto et al: Atmospheric rivers and associated precipitation patterns during the ACLOUD and PASCAL campaigns near Svalbard (May–June 2017): case studies using observations, reanalyses, and a regional climate model, Atmos. Chem. Phys., 22, 441–463, https://doi.org/10.5194/acp-22-441-2022, 2022.

Zhang et al: Extending the Center for Western Weather and Water Extremes (CW3E) atmospheric river scale to the polar regions, The Cryosphere, 18, 5239–5258, https://doi.org/10.5194/tc-18-5239-2024, 2024.

A: Thank you, we have now cited the suggested studies.

L125-126: "; Viceto et al., 2022; Zhang et al., 2024"

Lines 145-150: "The presence of snow on ice, not allowed in OpenIFS, has also been shown to mitigate surface energy and near-surface air-temperature biases (Pithan et al., 2016). " – it is not clear how the presence of snow on ice is treated in the AOSCM – please include more details as this is an important parameter influencing surface fluxes (especially the surface albedo and netSW). Is it from observations or parameterized?

A: Snow thickness is initialized according to CMEMS reanalysis data. Initial values for snow thickness and other sea-ice properties are now given in Table 1 in the main manuscript. As stated above, the sea-ice layer is described by 2 vertical levels and 5 thickness categories while snow is represented by a singular layer on top of the sea-ice (**L145-147) .** The LIM3 halo-thermodynamic parameterizations are solved for all categories and levels. For more information on the sea ice model physics, we refer the reader to the LIM3 documentation ((Rousset et al., 2015).

The simulated surface albedo is, on average, 0.56 for the MIZ and 0.93 for the sea-ice region, which is reasonable considering the respective sea-ice concentrations of approximately 0.6 and 0.99. We note that, in mid March when our WAI of interest is taking place, the amount of solar radiation reaching the snow surface is relatively small. Therefore, net SW does not influence the surface energy budget immensely. Turbulent heat fluxes (sensible and latent), as well as the downwelling longwave radiation are much stronger contributors. The sensible and latent heat fluxes are computed according to the surface skin temperature which we keep constant in time by initializing the sea-ice and snow layers with larger heat contents (colder temperature values).

"

Table 1. Representative values for sea-ice and snow properties used in the coupled simulations.

	MIZ	ice
Sea-ice concentration	60 %	99 %
Ice thickness	0.90 m	2.1 m
Snow thickness	0.13 m	0.31 m
Skin temperature	~ -1.5 ^{o}C	~ -8 ^{o}C

"

Fig 3: For the flux plots, it should be indicated in the caption that the flux is positive towards the surface. For SW and LW fluxes – please specify in the caption that these are net fluxes.

A: Thank you, we added the sign convention for the fluxes in the caption. Fig. 3 caption: **"Fluxes are positive towards the surface."**

Fig 3 caption: "in terms of integrated specific water content " – suggestion to add "integrated"

A: Fixed.

Line 218: "On the western flank of the airmass, where the LWP is larger, less solar radiation reaches the surface.. " – the statement is not clear. As the plot is showing netSW radiation at the surface, a large impact over the perennial sea ice and MIZ is most probably explained by the high surface albedo and reflection of a large portion of the incoming SW flux. My earlier question – how the snow on sea ice is treated – is an important factor to consider also over the sea ice zones. However, it is not clear why the netSW flux sharply decreases from rather large values south of 70ºN to almost zero north of it and then stays around zero over the open ocean not changing much over sea ice. It will be useful to include also a map of the surface albedo together with downwelling SW and investigate processes controlling netSW in more detail (in the later section using AOSCM). Part of this can be probably explained by changing solar zenith angle however the differences across the 70ºN are too sharp.

A: The area covered by the warm-air intrusion, at the time of the event (March 12-14) receives roughly 7 to 11.4 hours of daylight, at the northernmost and southernmost point of the trajectories respectively. The maps in Figures 2 and 3 show how the different variables evolve in time, along the path of the advection. At 65° N and 12 UTC (which is also local time for the airmass since it is advected along the prime meridian) the surface receives a maximum SW of around 200 W m^{-2}. The airmass then travels 5 latitudinal degrees in 6 hours and reaches 70° N around sunset, when SW at the surface drops to 0. Solar radiation increases again around the MIZ area, but the flux at the surface is significantly smaller due to the zenith angle (~12 W m^{-2}) . We have added explanatory comments to the captions of Figures 2 and 3 to clarify the Lagrangian map visualization method, which should help readers interpret the figures more effectively.

Figures 2 and 3 were produced with ERA5 data. ERA5 is the combined product of IFS cy41r2 and assimilation of observations, including satellite radiance measurement. IFS cy41r2 does not allow snow on sea-ice but representation could be corrected during the assimilation process.

The Lagrangian map of the temporal evolution and spatial variability of albedo is attached below (Fig. AR2.4). Albedo is computed as $Sw_{surf}^{up}/Sw_{surf}^{down}$, therefore the night-time parts during the airmass transport are excluded.

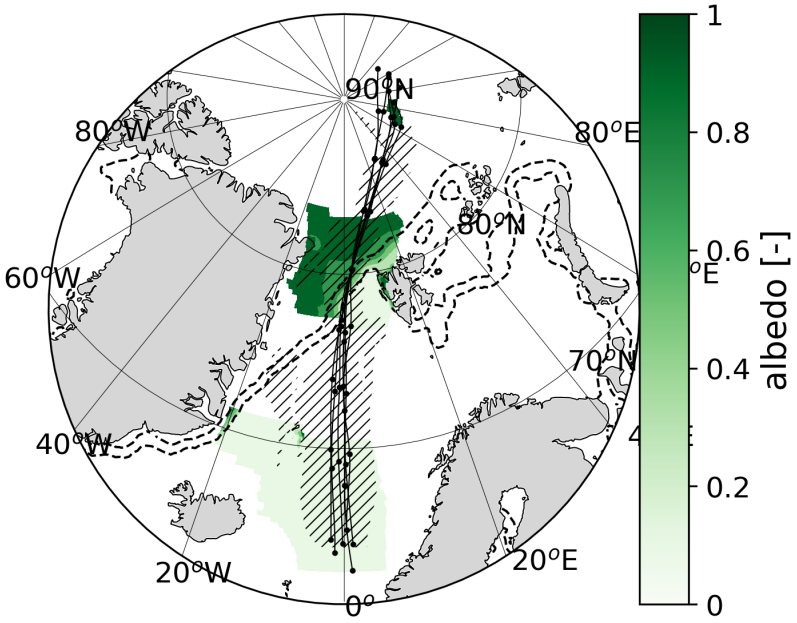

Figure AR2.4: Temporal evolution and spatial variability of the airmass during its poleward advection in terms of albedo. The trajectory ensemble is shown with black lines. Hatches mark the correlation range (see Sect. 2.3) around the airmass at each timestep. Square markers, when present, correspond to the observed values. Dashed contours show boundaries of the MIZ, corresponding to sea-ice concentration values ~~0~~**0.15** and ~~0.9~~**0.8** on March 13, at 12 UTC.

Lines 220-225: “The spatial variability in skin temperature over the ocean also appears to be controlling the exchange of latent heat at the surface (Fig. 3h). Over the warm ocean, the strongly negative (upward) fluxes indicate the ongoing moisture uptake by the airmass. “ : can you please clarify your interpretation. The upward LH flux indicates surface evaporation, which indeed seems to be related to the skin T according to the plots, while it is also strongly controlled by the near-surface winds and the boundary layer RH. To be sure that this evaporated moisture is taken by the air mass needs verification if the trajectory was within the boundary layer. Was this the case over the region with surface evaporation? It is anticipated that these questions are considered further when using AOSCM. Then the limitations of using ERA5 shall be stated clearly also highlighting the added value of modeling investigations. Boundary layer height is later shown in the AOSCM (Fig. 5) however the two sections (3.2 and 3.3.4) are somewhat disconnected.

See for example:

Sodemann, H.: The Lagrangian moisture source and transport diagnostic WaterSip V3.2, EGUsphere [preprint], https://doi.org/10.5194/egusphere-2025-574, 2025.

Sodemann, H., & Stohl, A. (2009). Asymmetries in the moisture origin of Antarctic precipitation. *Geophysical Research Letters*, **36**(22). **https://doi.org/10.1029/2009GL040242**

A: The lowest trajectory of the ensemble is within the boundary layer for the first 8 hours when surface evaporation is on-going. Therefore, this is a process that is relevant for this airmass transformation. Our modeling framework views the airmass as a a cohesive air column that is advected uniformly within the lowest 5 km, which makes the interaction with the surface relevant through the entire transformation, regardless of the position of the trajectories relative to the boundary layer top. We highlight the advantages of this modeling approach in the Introduction.

L75-76: "In this simple, novel framework we can investigate the physical drivers and timescales of the transformation, in isolation from the complex dynamics that are typically associated with warm-air intrusions."

Further downstream the boundary layer becomes shallower and the airmass is lifted by a large-scale updraft, becoming progressively more decoupled from the surface (Fig. AR2.5). In reality when that happens, low-level convergence should bring new airmasses into the column through horizontal advection, which is something that our modeling framework does not take into account. This is already discussed as a limitation to the Lagrangian AOSCM but will be stated more clearly in the conclusions.

L538-539: "It is important to note that the large-scale updrafts applied in our simulations would normally be accompanied by low-level convergence and, therefore, advection of new air in the column which is prohibited in our framework."

We plan to explore the importance of the complex dynamic conditions during warm-air intrusions (WAIs) in greater detail in future work using this Lagrangian modeling framework.

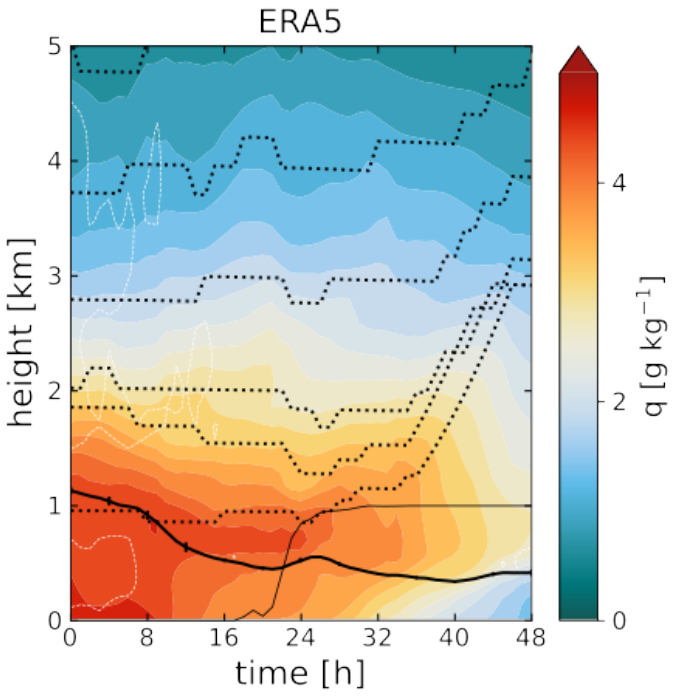

Figure AR2.5: Time-height cross-sections of the ensemble average specific humidity from ERA5. Dotted lines represent the height of the trajectories. The thick solid line shows the evolution of the

boundary layer height during the airmass transformation. The thin solid line marks the along-stream sea-ice concentration.

Section 3.3.3: I suggest including a reference to Fig. 4 to make it clear the results are based on this figure

A: Added figure reference in **L317**.

Lines 300-305: "The uncertainty range ERA5 and IFS-OF curves grows larger due to the slight divergence of the trajectory ensemble. " – I am not sure to follow this interpretation. My understanding from reading the methodology is that the trajectories are the same, while thermodynamics state is represented by 3 different models (ERA5, IFS-OF and AOSCM). Thus, this is not the divergence of the trajectory ensemble but shall be explained by the differences in the model physics and processes representation. Could you please clarify and rephrase the statement.

A: We apologize for the confusing phrasing here. With the term "uncertainty range" we do not refer to the differences between ERA5 and IFS-OF which, as the reviewer points out, would be the result of differences in model physics and assimilation of observations. "Uncertainty range" in Fig. 4 are the perpendicular faded line that show the variability in the thermodynamic state within the trajectory ensemble in each dataset. For ERA5 and IFS-OF that range shrinks around the MIZ over which the trajectories were initialized and their in-between distances are the smallest. As the trajectories spread out towards the northernmost and southernmost end, they span a larger area and captures more of the airmass variability making the uncertainty range around the ensemble mean grow.

We rephrase:

L325: "~~The uncertainty range ERA5 and IFS-OF curves grows larger~~ The uncertainty ranges around the ERA5 and IFS-OF curves grow larger"

Fig 5: Please indicate the time 0 (2/03/2022, 00UTC) in the caption

A: Added **"The time axis is in hours since 12/03/2022, 12UTC."** in the caption.

Line 355: "Over the MIZ, the subsidence spikes abruptly and over the sea-ice leg the vertical motion is predominantly upward, with ω increasing the deeper the airmass intrudes into the Arctic. ": is this updraft driven by cloud top radiative cooling (as described in Morrison et al 2012)? This can be seen in Fig. 7a discussed later in section 3.3.6.

Morrison, H., de Boer, G., Feingold, G. *et al*. Resilience of persistent Arctic mixed-phase clouds. *Nature Geosci* **5**, 11–17 (2012). https://doi.org/10.1038/ngeo1332

A: The AOSCM is forced with ERA5 vertical velocities (ω) shown in Fig. 5 (s-t) in the main manuscript. Therefore, these updrafts represent large-scale motions that can not be resolved in the single-column format and are therefore prescribed. In order to isolate the cloud ascent caused by the

model physics we would need to deactivate vertical advection (Fig. AR2.6). The ascent of the top cloud layer is much slower and, in the absence of adiabatic cooling, weaker changes in the heat and moisture content of the airmass in total. This is an interesting aspect of the transformation and, although it is outside of the scope of this study, we plan to investigate it further in our future Lagrangian AOSCM applications.

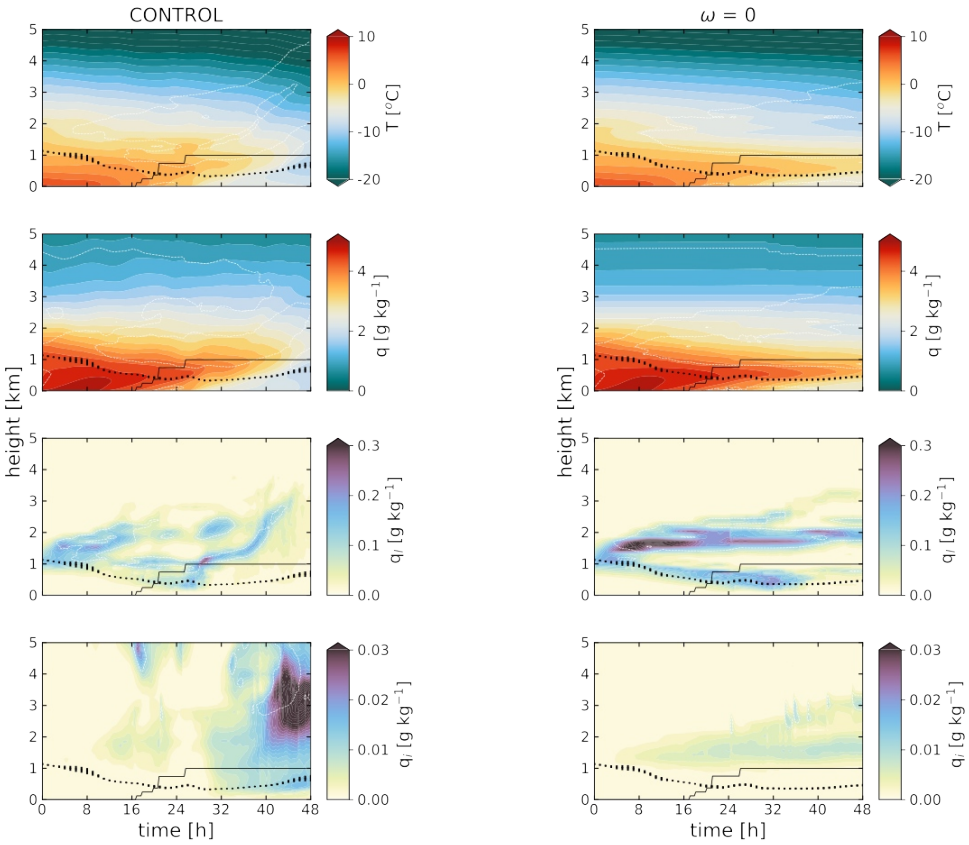

Figure AR2.6: Time-height cross-sections of the ensemble average temperature (1st row from the top), specific humidity (2nd row), specific liquid (3rd row) and ice water (4th row). The left column shows the AOSCM simulations as presented in the manuscript and the right column shows experiments with vertical advection switched off (ω = 0).

To make more emphasis on the process understanding I suggest to move section 3.3.5 "Comparison with observed transformation" before section 3.3.4 – this will show how each model represents each parameter before investigating the evolution in these parameters. Further, it will be beneficial to combine sections 3.3.4 "Vertical structure" with section 3.3.6 "Physical and dynamical drivers" explaining the drivers (Fig. 7) right away when presenting the vertical structure transformations (Fig. 5).

A: We think the discussion of vertical structure Sect. 3.3.4 is a more natural continuation of Sections 3.3.[1-3] that describe the transformation in bulk terms. Sect. 3.3.5 then focuses on the smaller areas of the cross-sections where observations are available. It is, in our opinion, preferable to present the airmass transformation in its entirety before focusing on the specific points where observations are available.

Section 3.3.5: As cloud ice and liquid content are key drivers of the radiative fluxes and updrafts, can the authors also include cloud evaluation, eg with cloud LWP from HAMP onboard HALO? I understand that this can be beyond the scope of the paper but if the data are already available this will be beneficial to see how AOSCM represents cloud properties.

A: Thank you for raising this point. LWP retrievals from HAMP were still a work in progress when this manuscript was submitted but are now available. We are pleased at the opportunity to include them in our plots. We have incorporated the observed LWP values in AR2.7 (Fig 3b in the manuscript).

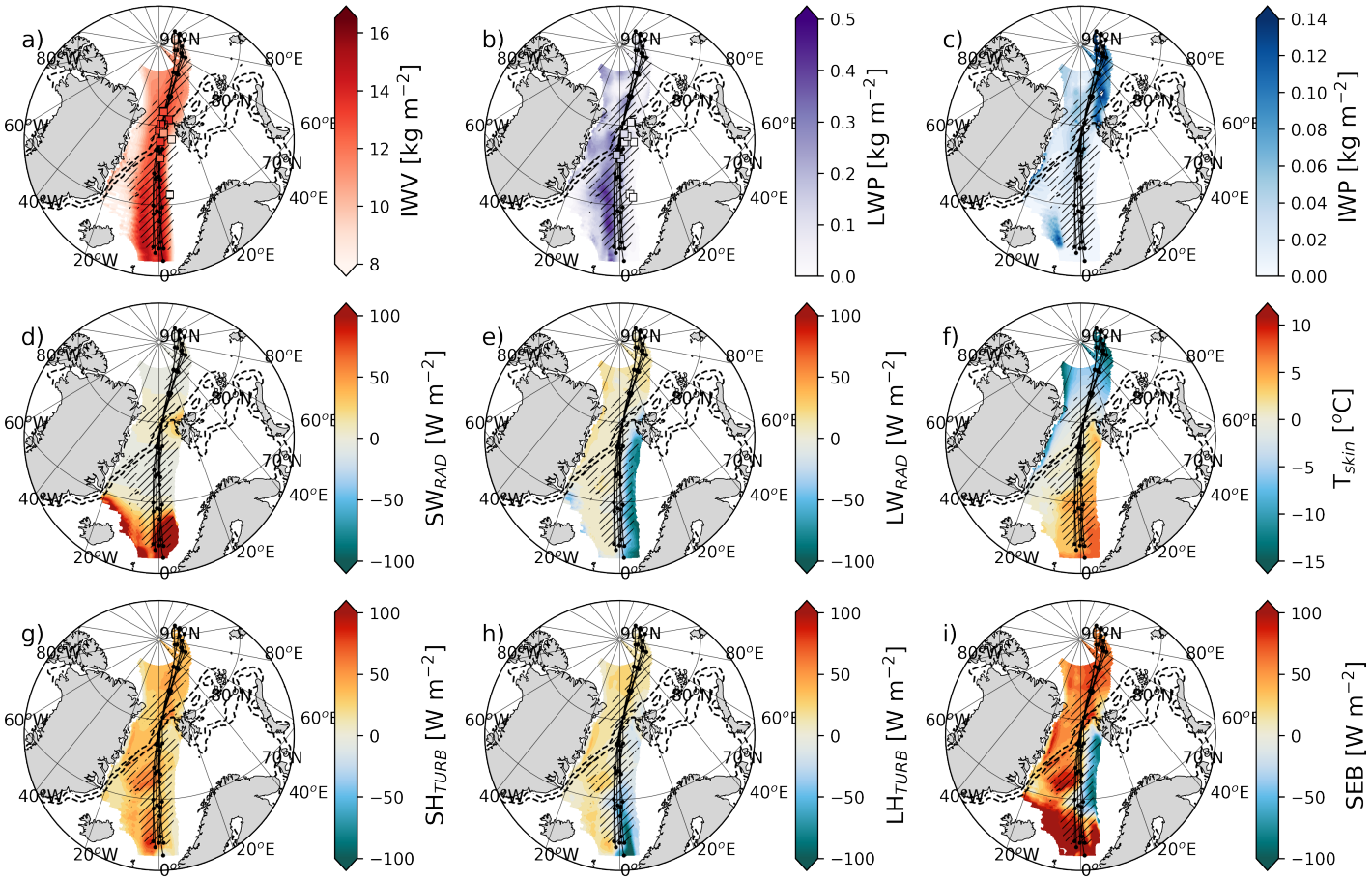

Figure AR2.7: Same as Fig. 3 but with LWP retrievals based on HAMP observations included in Fig. 3b.

We offer a description of the dataset in Sect. 2.1 and discuss the results in:

L238-241: "The observed spatiotemporal cloud distribution is similar to ERA5. ERA5 shows a positive LWP bias (-0.03 kg m^{-2} on average) in the east sector of the airmass, where the cloud is thin, and a negative LWP bias (-0.04 kg m^{-2} on average) in the west where thicker clouds are encountered. The biases are larger than estimated uncertainty of the LWP retrieval (0.02 kg m^{-2})."

Minor edits:

Line 168 : "of a strong cyclone" - add 'a'

A: Fixed.

Throughout the text – spaces missing at multiple places

A: We skimmed the text and added missing spaces.

References

1. ECMWF: IFS Documentation – Cy43r3, ECMWF, https://doi.org/10.21957/efyk72kl, dOI: 10.21957/efyk72kl, 2017.
2. Ehrlich, A., Crewell, S., Herber, A., Klingebiel, M., Lüpkes, C., Mech, M., Becker, S., Borrmann, S., Bozem, H., Buschmann, M., Clemen, H.-C., De La Torre Castro, E., Dorff, H., Dupuy, R., Eppers, O., Ewald, F., George, G., Giez, A., Grawe, S., Gourbeyre, C., Hartmann, J., Jäkel, E., Joppe, P., Jourdan, O., Jurányi, Z., Kirbus, B., Lucke, J., Luebke, A. E., Maahn, M., Maherndl, N., Mallaun, C., Mayer, J., Mertes, S., Mioche, G., Moser, M., Müller, H., Pörtge, V., Risse, N., Roberts, G., Rosenburg, S., Röttenbacher, J., Schäfer, M., Schaefer, J., Schäfler, A., Schirmacher, I., Schneider, J., Schnitt, S., Stratmann, F., Tatzelt, C., Voigt, C., Walbröl, A., Weber, A., Wetzel, B., Wirth, M., and Wendisch, M.: A comprehensive in situ and remote sensing data set collected during the HALO–(AC)3 aircraft campaign, Earth System Science Data, 17, 1295–1328, https://doi.org/10.5194/essd-17-1295-2025, publisher: Copernicus GmbH, 2025.
3. Pithan, F., Ackerman, A., Angevine, W. M., Hartung, K., Ickes, L., Kelley, M., Medeiros, B., Sandu, I., Steeneveld, G.-J., Sterk, H. a. M., Svensson, G., Vaillancourt, P. A., and Zadra, A.: Select strengths and biases of models in representing the Arctic winter boundary layer over sea ice: the Larcform 1 single column model intercomparison, Journal of Advances in Modeling Earth Systems, 8, 1345–1357, https://doi.org/10.1002/2016MS000630, _eprint: https://onlinelibrary.wiley.com/doi/pdf/10.1002/2016MS000630, 2016.
4. Rousset, C., Vancoppenolle, M., Madec, G., Fichefet, T., Flavoni, S., Barthélemy, A., Benshila, R., Chanut, J., Levy, C., Masson, S., and Vivier, F.: The Louvain-La-Neuve sea ice model LIM3.6: global and regional capabilities, Geoscientific Model Development, 8, 2991–3005, https://doi.org/10.5194/gmd-8-2991-2015, publisher: Copernicus GmbH, 2015.
5. Vaisala: Vaisala Radiosonde RD41 datasheet in English, https://www.nirb.ca/portal/dms/script/dms_download.php?fileid=340414&applicationid=125718&sessionid=ka7asjkahsplnt1tq4rduoqbl1, accessed: 2025-03-24, 2020.
6. Viceto, C., Gorodetskaya, I. V., Rinke, A., Maturilli, M., Rocha, A., and Crewell, S.: Atmospheric rivers and associated precipitation patterns during the ACLOUD and PASCAL campaigns near Svalbard (May–June 2017): case studies using observations, reanalyses, and a regional climate model, Atmospheric Chemistry and Physics, 22, 441–463, https://doi.org/10.5194/acp-22-441-2022, publisher: Copernicus GmbH, 2022
7. Zhang, Z., Ralph, F. M., Zou, X., Kawzenuk, B., Zheng, M., Gorodetskaya, I. V., Rowe, P. M., and Bromwich, D. H.: Extending the Center for Western Weather and Water Extremes (CW3E) atmospheric river scale to the polar regions, The Cryosphere, 18, 5239–5258, https://doi.org/10.5194/tc-18-5239-2024, publisher: Copernicus GmbH, 2024.